Available online at www.sciencedirect.com
SCIENCE DIRECT®
Journal of Organometallic Chemistry 691 (2006) 1402–1410
Journal of Organometallic Chemistry
www.elsevier.com/locate/jorganchem

Dimeric allylpalladium(II) complexes with pyrazolate bridges: Synthesis, characterization, structure and thermal behaviour

A. Singhal [a], R. Mishra [a], S.K. Kulshreshtha [a,*], Paul V. Bernhardt [b], Edward R.T. Tiekink [c]

[a] Chemistry Division, Bhabha Atomic Research Centre, Trombay, Mumbai, Maharashtra 400 085, India
[b] School of Molecular and Microbial Sciences, University of Queensland, Brisbane 4072, Qld, Australia
[c] Department of Chemistry, The University of Texas at San Antonio, San Antonio, TX 78249-0698, USA

Received 9 November 2005; received in revised form 6 December 2005; accepted 13 December 2005
Available online 20 January 2006

Abstract

The synthesis, characterization and thermal behaviour of some new dimeric allylpalladium (II) complexes bridged by pyrazolate ligands are reported. The complexes $[Pd(\mu\text{-}3,5\text{-}R'_2pz)(\eta^3\text{-}CH_2C(R)CH_2)]_2$ [R = H, R′ = $CH(CH_3)_2$ (**1a**); R = H, R′ = $C(CH_3)_3$ (**1b**), R = H, R′ = CF_3 (**1c**); R = CH_3, R′ = $CH(CH_3)_2$ (**2a**); R = CH_3, R′ = $C(CH_3)_3$ (**2b**); and R = CH_3, R′ = CF_3 (**2c**)] have been prepared by the room temperature reaction of $[Pd(\eta^3\text{-}CH_2C(R)CH_2)(acac)]$(acac = acetylacetonate) with 3,5-disubstituted pyrazoles in acetonitrile solution. The complexes have been characterized by NMR (^1H, $^{13}C\{^1H\}$), FT-IR, and elemental analyses. The structure of a representative complex, viz. **2c**, has been established by single-crystal X-ray diffraction. The dinuclear molecule features two formally square planar palladium centres which are bridged by two pyrazole ligands and the coordination of each metal centre is completed by allyl substituents. The molecule has non-crystallographic mirror symmetry. Thermogravimetric studies have been carried out to evaluate the thermal stability of these complexes. Most of the complexes thermally decompose in argon atmosphere to give nanocrystals of palladium, which have been characterized by XRD, SEM and TEM. However, complex **2c** can be sublimed in vacuo at 2 mbar without decomposition. The equilibrium vapour pressure of **2c** has been measured by the Knudsen effusion technique. The vapour pressure of the complex **2c** could be expressed by the relation: $\ln(p/\text{Pa})(\pm 0.06) = -18047.3/T + 46.85$. The enthalpy and entropy of vapourization are found to be 150.0 ± 3 kJ mol^{-1} and 389.5 ± 8 J K^{-1} mol^{-1}, respectively.

Keywords: η^3-Allylpalladium complexes; Pyrazolate ligands; NMR spectroscopy; X-ray crystal structure; Transmission electron microscopy

1. Introduction

Thin films of palladium find many applications in electronic industry, such as electrical contacts (replacing gold), multi-layer magneto-optical data storage materials, hydrogen sensors or infrared-sensors, multilayer chip capacitors, and electrode coating materials [1]. They are also useful as catalysts for a variety of gas-phase reactions [2] and membrane materials for gas separation [3]. Nano-sized palladium particles deposited on suitable substrates find wide applications in heterogeneous catalysis [4]. Thus, there has been significant interest in developing suitable precursor molecules for the chemical vapour deposition (CVD) of palladium thin films and nanoparticles. The lability of the allyl groups in allylpalladium compounds is well documented and complexes such as $Pd(\eta^3\text{-allyl})_2$, $[Pd(\eta^3\text{-}CH_2CHCHMe)_2]$ and $[C_pPd(\eta^3\text{-allyl})]$ have proven to be excellent precursors for the deposition of high-purity palladium thin films by thermal CVD [5]. However, these complexes suffer from low thermal- and air-stability. Recently, complexes of the type (η^3-allyl)(β-diketonato)palladium(II) [6] and (η^3-allyl)(β-diketoiminato)palladium(II) [7] which exhibit excellent thermal stability and volatility have been reported.

Pyrazolato ligands are an interesting group of ligands [8] whose coordination chemistry with transition and

* Corresponding author. Tel.: +91 22 25593829; fax: +91 22 25505151.
E-mail addresses: kulshres@magnum.barc.ernet.in (S.K. Kulshreshtha), Edward.Tiekink@utsa.edu (E.R.T. Tiekink).

0022-328X/$ - see front matter © 2005 Elsevier B.V. All rights reserved.
doi:10.1016/j.jorganchem.2005.12.037

non-transition metals has been thoroughly reviewed [9]. These ligands can be easily prepared and their properties can be suitably modified by appropriate choice of the carbon-bound substituents. In particular, 3,5-disubstituted derivatives such as 3,5-di-*tert*-butyl- [10,11] and 3,5-bis(trifluoromethyl)-pyrazolate [12] are known to impart increased volatility to their metal complexes. Further, pyrazolates, being nitrogen donor ligands, are more basic than common oxygen donor ligands, such as β-diketonate and can therefore bind strongly to metal centres resulting in source compounds with enhanced stability. With these considerations, we have investigated the chemistry and thermal behaviour of a series of pyrazolato-bridged dimeric allylpalladium complexes, $[Pd(\mu\text{-}3,5\text{-}R'_2pz)(\eta^3\text{-}CH_2C(R)\text{-}CH_2)]_2$ (R = H (**1**)) or CH_3 (**2**) R′ = ($CH(CH_3)_2$, $C(C\text{-}H_3)_3$, CF_3). The complex $[Pd(\mu\text{-}3,5\text{-}(CF_3)_2pz)(\eta^3\text{-}C_3H_5)]_2$ (**1c**) has recently been reported by Jones et al. [12] and was obtained by reacting $[Pd(\mu\text{-}Cl)(\eta^3\text{-}C_3H_5)]_2$ with 3,5-$(CF_3)_2$pzLi at room temperature for 12 h. In this work, we report a faster and convenient method to synthesize pyrazolato-bridged dimeric allylpalladium(II) complexes, their characterization and thermal stability, and in the case of **2c**, equilibrium vapour pressure measurements.

2. Results and discussion

2.1. Synthesis and characterization of the complexes

The complexes, $Pd(\mu\text{-}3,5\text{-}R'_2pz)(\eta^3\text{-}CH_2C(R)CH_2)]_2$ R = H or CH_3; R′ = ($CH(CH_3)_2$, $C(CH_3)_3$, CF_3) are prepared in high-yields from the reaction of the appropriate pyrazole with the complex, $[Pd(acac)(\eta^3\text{-}CH_2C(R)CH_2)$ (generated in situ by the reaction between the chloro-bridged allylpalladium dimer and thallium(I)acetylacetonate) (Scheme 1). The *acac* method reported by us represents a general and convenient synthetic approach to synthesize several new dimeric allylpalladium(II) complexes with different bridging ligands [13]. Most of the complexes are air-stable solids and can be stored at room temperature for long periods. However, complexes **1b** and **2b** tend to decompose if kept in air at room temperature for long periods and have to be stored under argon below 0 °C. All complexes are white to off-white solids and have been characterized by ^1H, $^{13}C\{^1H\}$ NMR, FTIR, and C, H, N analyses.

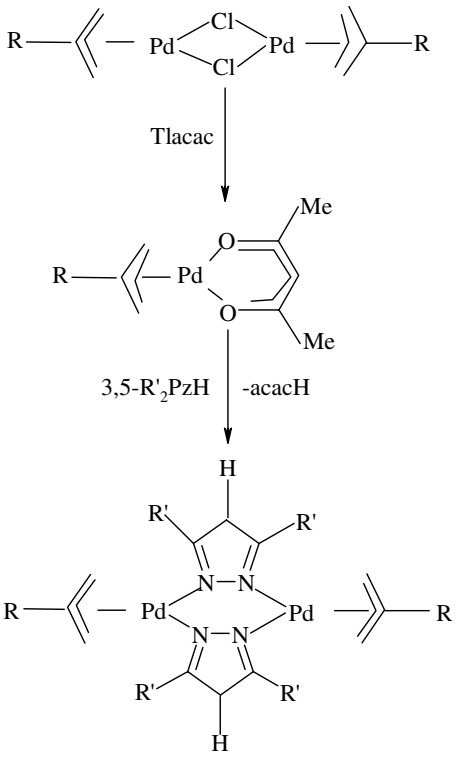

	1a	1b	1c	2a	2b	2c
R	H	H	H	CH_3	CH_3	CH_3
R'	Pr^i	Bu^t	CF_3	Pr^i	Bu^t	CF_3

Scheme 1.

2.2. NMR of allylpalladium complexes

The room temperature ^1H NMR spectra of the complexes **1** and **2** were complex but showed the correct proton ratios for both ligands. For example, in complexes **1a** and **1c** four sets of resonances each for *anti* and *syn* protons with both showing up as doublets (*anti* J_{HH} = ~12 Hz, *syn* J_{HH} = ~7 Hz) are observed. Two/three multiplets appeared for the proton bound to central carbon atom of the allyl ligand. The three resonances between 5.8 and 6.8 ppm are attributed to the single proton bound to C-4 of the pyrazolate ring. For complexes, **2a** and **2c** two sets of resonances each for *anti*, *syn* and methyl groups were observed. These data suggest that for these complexes in solution a mixture of isomers are present. Of relevance here is the proton NMR data for the original series of dinuclear palladium(II) allyl derivatives of dimethylpyrazolate or of the parent pyrazolate reported by Trofimenko [14]. For these complexes also, the ^1H NMR spectra were found to be more complex than those expected for a molecule of simple C_{2v} symmetry. It was proposed that the NMR data were compatible with a mixture of conformational isomers resulting from different orientations of the allyl groups which may arise due to the formal rotation of allyl groups, inversion of the entire metallocycle or the presence of isomer **I** (Fig. 1). Of the different conformational isomers possible, structure **I** has each set of *syn* and *anti* protons in a different environment and the left- and right-side R′ groups are also non-equivalent. Both structures **II** and **III** have C_{2v} symmetry. The room temperature spectra of **1a** and **1c** would be compatible with either **I** or a 1:1 mixture of **II** and **III**. The latter possibility looks less attractive as the putative steric interactions between the R groups would disfavour structure

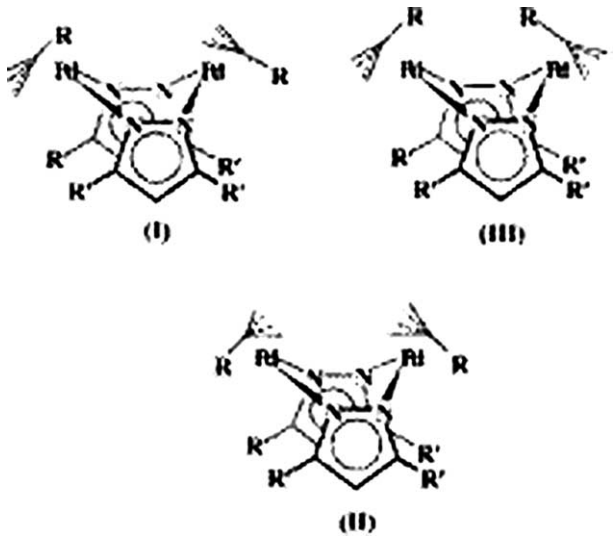

Fig. 1. Conformational isomers possible for $[Pd(\mu\text{-}3,5\text{-}R'_2pz)(\eta^3\text{-}CH_2C(R)CH_2)]_2$. (Reprinted from Ref. [12] with permission from Elsevier and Ref. [14] with permission from American Chemical Society.)

III and even if it did exist, it is unlikely that it would exist in an exactly 1:1 ratio with **II**.

2.3. Crystallography

The molecular structure of **2c** is shown in Fig. 2 from which it can be seen that the dimeric complex features two bidentate bridging pyrazolate ligands. These form experimentally equivalent Pd–N bond distances in the range 2.100(2)–2.108(2) Å. The formally square planar coordination geometry for each palladium centre is completed by an allyl group. Key bond lengths and bond angles are given in Table 1. The Pd–C separations are equal at the 5σ level, falling in the range 2.103(3)–.129(3) Å, with the longer separation in each case being formed by the palladium atom and the central carbon atom of each allyl group. In terms of the possible isomers represented in

Table 1
Selected bond lengths (Å) and angles (°) for **2c**

Bond lengths			
Pd(1)–N(1a)	2.100(2)	Pd(2)–N(2a)	2.100(2)
Pd(1)–N(1b)	2.108(2)	Pd(2)–N(2b)	2.105(2)
Pd(1)–C(1)	2.103(3)	Pd(2)–C(5)	2.114(3)
Pd(1)–C(2)	2.120(3)	Pd(2)–C(6)	2.129(3)
Pd(1)–C(3)	2.113(3)	Pd(2)–C(7)	2.115(3)
Bond angles			
N(1a)–Pd(1)–N(1b)	89.17(9)	N(2a)–Pd(2)–N(2b)	88.42(9)
N(1a)–Pd(1)–C(1)	101.42(12)	N(2a)–Pd(2)–C(5)	101.31(12)
N(1a)–Pd(1)–C(2)	132.96(12)	N(2a)–Pd(2)–C(6)	133.75(11)
N(1a)–Pd(1)–C(3)	169.20(12)	N(2a)–Pd(2)–C(7)	168.82(12)
N(1b)–Pd(1)–C(1)	169.35(12)	N(2b)–Pd(2)–C(5)	169.18(12)
N(1b)–Pd(1)–C(3)	101.52(12)	N(2b)–Pd(2)–C(6)	134.43(11)
N(1b)–Pd(1)–C(2)	132.46(12)	N(2b)–Pd(2)–C(7)	101.90(11)
C(1)–Pd(1)–C(2)	38.71 (14)	C(5)–Pd(2)–C(6)	38.58(13)
C(1)–Pd(1)–C(3)	67.87(14)	C(5)–Pd(2)–C(7)	68.06(14)
C(2)–Pd(1)–C(3)	38.33(13)	C(7)–Pd(2)–C(6)	38.48(13)

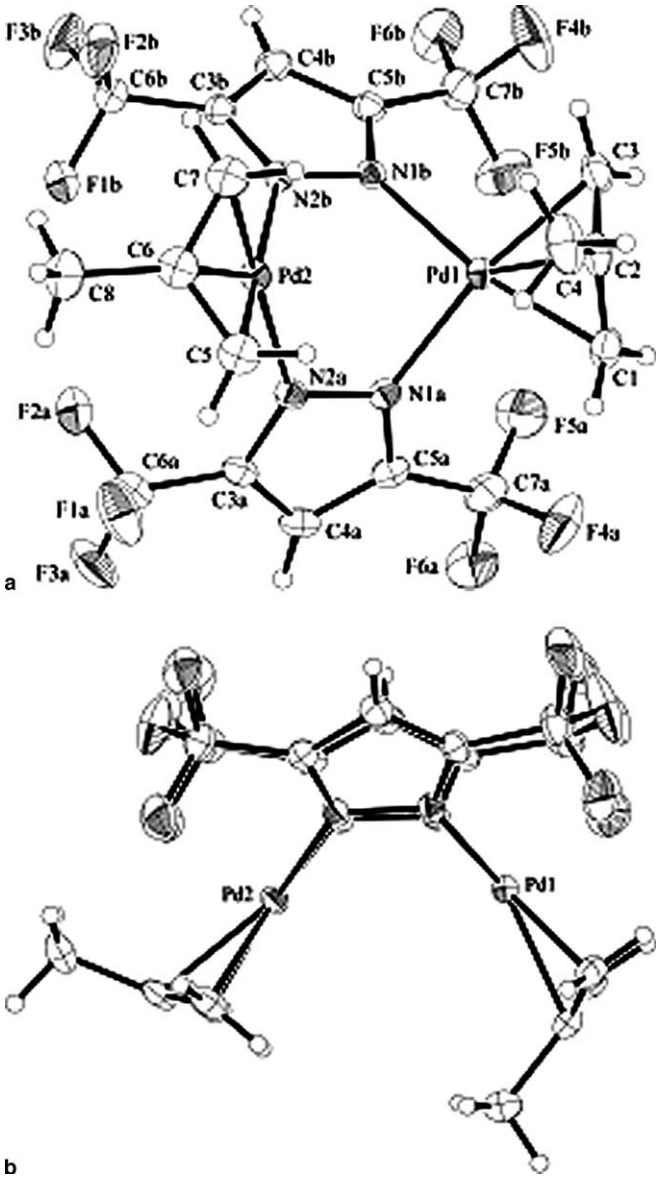

Fig. 2. The molecular structure of **2c** showing (a) the atomic numbering scheme and (b) a side view highlighting the disposition of the pyrazolate ligands.

Fig. 1, the molecular structure of **2c** adopts the conformation in which the allyl groups have an opposite orientation with respect to the Pd_2N_4 core, i.e., isomer **I**, as emphasised in the lower view of Fig. 2b. The molecule adopts a boat conformation as seen in the dihedral angles between the two allyl groups (ca. 75°) and the two five-membered rings (ca. 83°). This conformation found for **2c** has also been reported for the previously described structure of **1c** [12]. Indeed, the geometric parameters reported for **1c** are in good agreement to those reported above, i.e., the ranges of Pd–N and Pd–C are 2.101(3)–2.111(3) Å and 2.099(4)–2.133(4) Å, respectively. In a closely related structure, i.e., $[Pd(\mu\text{-}3,5\text{-}Me_2pz)(\eta^3\text{-}CH_2C(H)CH_2)]_2$ [15] the molecule has a configuration comparable to that shown as isomer **II** in Fig. 1. A partial crystallographic analysis was also conducted on complex **1b** but problems in modelling the

Table 2
TGA data for $[Pd(\mu\text{-}3,5\text{-}R'_2pz)(\eta^3\text{-}CH_2C(R)CH_2)]_2$

Compound	Step I		Step II	
	Temp. range (°C)	% wt. loss[a]	Temp. range (°C)	% wt. loss
1a	175–269	13.5 (13.7)	269–406	51.5 (50.6)
1b	97–169	11.7 (12.5)	171–260	55.8 (54.9)
1c	160–260	89.9	–	–
2a	200–265	19.7 (17.6)	280–380	49.5 (49.6)
2b	160–204	17.4 (16.2)	206–227	51.2 (52.6)
2c	166–284	100	–	–

[a] The values in parentheses correspond to expected weight loss.

significant disorder precluded a full report (see Section 4). However, despite this difficultly, the molecular connectivity was established unambiguously. The essential molecular structure is as described above with the notable exception of the relative orientation of allyl groups which correspond to the conformation represented as isomer **II** in Fig. 1. This observation underscores the inherent flexibility in these systems with respect to the orientations of the allyl groups to the Pd_2N_4 cores of the complexes.

2.4. TG analysis

The thermogravimetric analyses (TGA) of $[Pd(\mu\text{-}3,5\text{-}R'_2pz)(\eta^3\text{-}CH_2C(R)CH_2)]_2$ were carried out in flowing argon atmosphere and the results are summarized in Table 2. The typical TG plots for two representative complexes (**1a** and **2c**) are shown in Fig. 3. From TG analysis it was found that most of the dimeric allyl complexes with pyrazolate bridges (i.e., **1a**, **1b**, **2a**, and **2b**) decomposed in two steps to leave a residue of metallic palladium, with the mass loss in the first step corresponding to the loss of the allyl moieties and the mass loss in the second step corresponding to the loss of pyrazolate groups. The mass loss obtained from TGA agrees well within experimental error with the calculated mass loss for each step for all the above complexes (cf. Table 2). However, complex **1c**, containing the 3,5-bis(trifluromethyl) pyrazolate ligand, partly evaporated and partly decomposed (~90% evaporation was observed) leaving a very small amount of metallic Pd residue. The TGA of **2c** is of particular interest as it showed a simple one-step loss of nearly 100% within the temperature range (166–280 °C) (Fig. 3b). This observation is consistent with highly effective transportation of palladium metal into the gas phase without decomposition. The enthalpy and entropy of evaporation for **2c** has been determined. From the data collected in Table 2, the stabilities of the complexes can be arranged in the following order:

1b < **1a** < **1c** and **2b** < **2a** < **2c**.

2.5. Vapour pressure measurements

The thermogravimetric (TG) plot of **2c** (Fig. 3b) showed that the complex congruently vapourizes above 439 K in a single step. No break in the TG plot for the decomposition of the complex was seen. NMR (^1H, $^{13}C\{^1H\}$), FT-IR and melting point data for the residue of the partially evaporated sample obtained from the Knudsen effusion studies showed the presence of the original complex. The NMR spectra (^1H, $^{13}C\{^1H\}$) of the condensed phase deposited on the cooler part of the reaction tube showed the presence

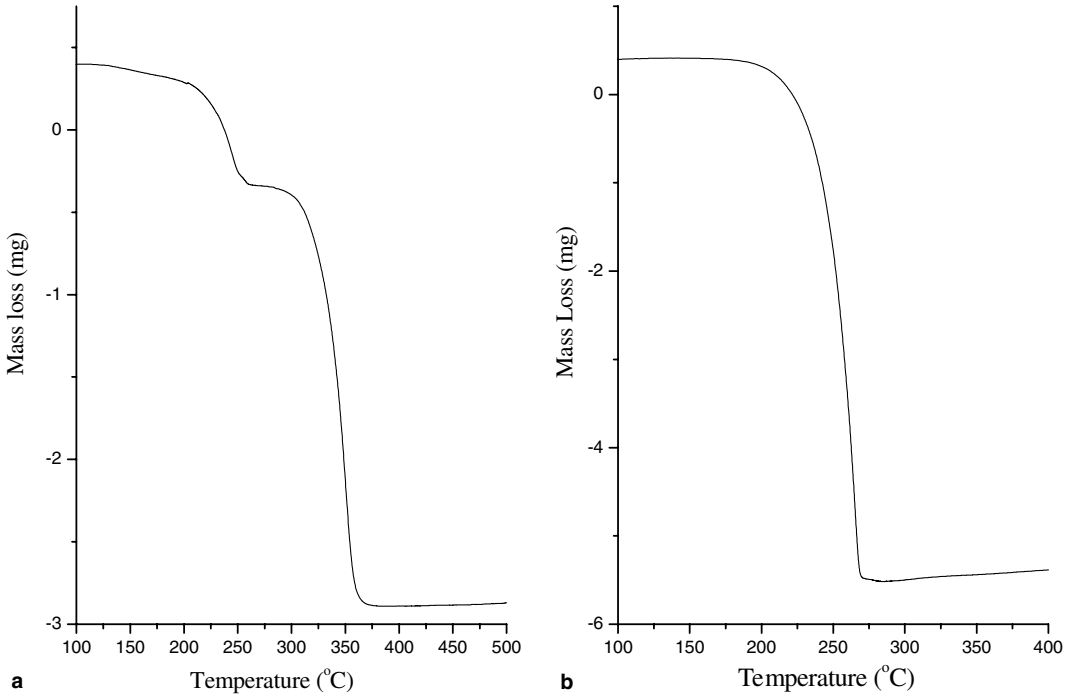

Fig. 3. TGA traces for: (a) **1a** (initial weight: 4.95 mg) which decomposed in two steps leaving a 35% residue; and (b) **2c** (initial weight: 5.9 mg) which showed 100% evaporation between 166 and 284 °C.

of pure **2c**. This is indicative of the fact that the chemical composition of the complex is retained after the reaction and that the vapourization process is congruent.

The isothermal rate of effusion of the vapours from the orifice was obtained from the observed total mass loss over a time, t, at steady state. The vapour pressure of **2c** in the Knudsen cell was derived from the mass loss/time data using the relation of effusive flow obtainable from the kinetic theory of gases applied to vapour fluxes. The following relation then expresses the vapour pressure of **2c** (g) in terms of the mass loss m:

$$p = (1/A) \times 1/K_c \times (m/t) \times (2\pi RT/M)^{1/2} \quad (1)$$

In this equation, p is the vapour pressure of the complex, A is the orifice area, K_c is the Clausing factor, T is the absolute temperature in Kelvin, M is the molecular weight of complex (729.15), and R is the universal gas constant. In the present experiment for thin knife edge orifice, K_c was taken to be 1.

The vapour pressure of **2c** in the temperature range 359–385 K as calculated from experimentally determined parameters involved in the above equation are given in Table 3 for all the experimental runs. The linear least-squares fit of ln (p) versus $1/T$ is given in Fig. 4. The least-square fitted equation is represented as:

Table 3
Vapour pressure data for **2c**

Temp (K)	Time (s)	Mass loss (μg)	Pressure (Pa)
359	240	285	0.034
364	240	64	0.065
374	240	19	0.222
377.5	240	10	0.394
381	240	174	0.610
385	240	113	1.004

$$\ln(p/\mathrm{Pa}) \pm 0.06 = -18047.3/T + 46.85 (359 \leqslant T/\mathrm{K} \leqslant 385). \quad (2)$$

The slope and intercept of the linear equation gave the values of mean molar enthalpy and entropy, respectively, for the vapourization of the compound. The values of enthalpy and entropy were found to be 150.0 ± 3 kJ mol^{-1} and 389.5 ± 8.0 J K^{-1} mol^{-1}, respectively.

2.6. Thermal decomposition of the complexes

Thermolysis of the complexes **1b** and **2b** in refluxing xylene and of complexes **1a** and **2a** at 500 °C at a rate of 5 °C min^{-1} in a furnace under an argon atmosphere were carried out and nanocrystals of palladium metal were obtained in each case. X-ray diffraction patterns of the nanocrystals revealed broad reflections which compared well with the pattern reported for palladium metal [16]. Fig. 5 shows the XRD spectra of the powders obtained from thermolysis of **1b**, **2a**, and **2b**. The average crystallite size of 5.4 ± 0.2 nm was estimated with the Scherrer equation for the nanocrystals derived from complexes. The surface morphology of the nanoparticles obtained after thermolysis of complex **2b** was determined by high-resolution scanning electron micrographs (SEM) and transmission electron microscopy (TEM). While SEM analyses showed spherically shaped aggregates of palladium with more or less uniform size of 0.5 μm with very small distribution (Fig. 6), TEM analyses revealed spherical nanoparticles having mean diameters in the range 5–12 nm (Fig. 7). The method represents a facile synthetic procedure to produce palladium nanoparticles at moderately low temperature. Kim et al. [17] have earlier obtained palladium nanoparticles with particle sizes of 3.5, 5, and 7 nm from the thermal decomposition of

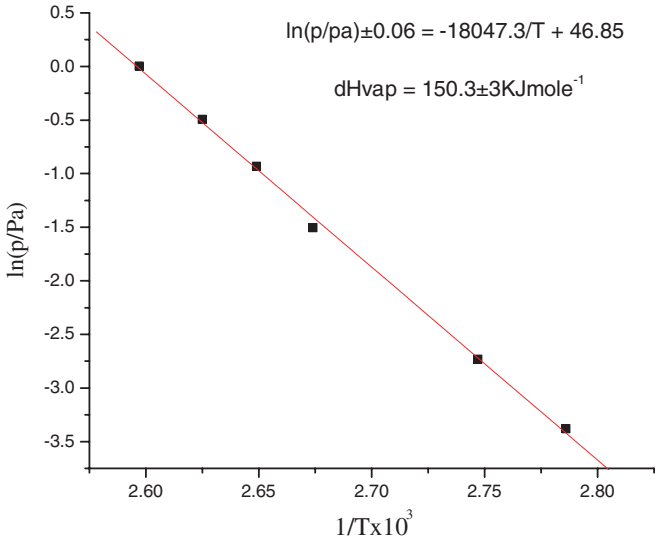

Fig. 4. Graph showing the relationship between vapour pressure and temperature for the complex **2c**.

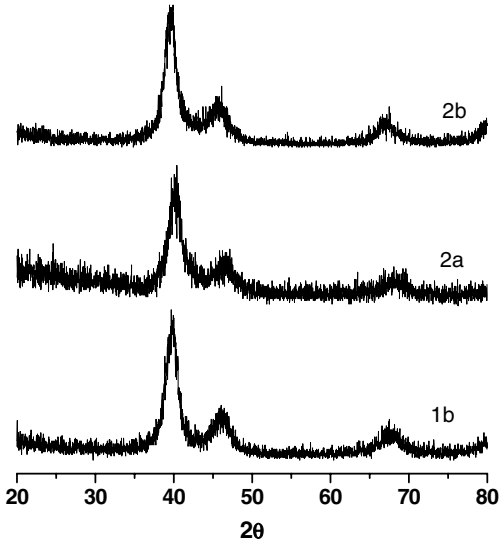

Fig. 5. X-ray diffraction spectra for the nanocrystals obtained after thermolysis of complexes **1b**, **2a** and **2b**.

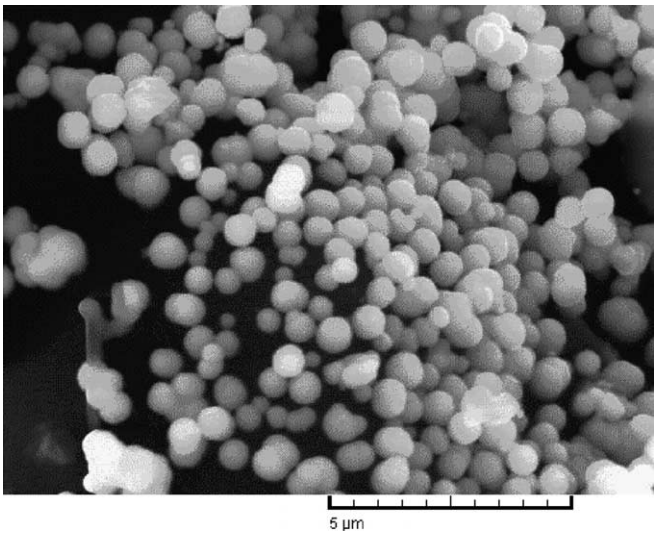

Fig. 6. Scanning electron micrograph of the nanocrystals derived from thermolysis of complex **2b** in refluxing xylene.

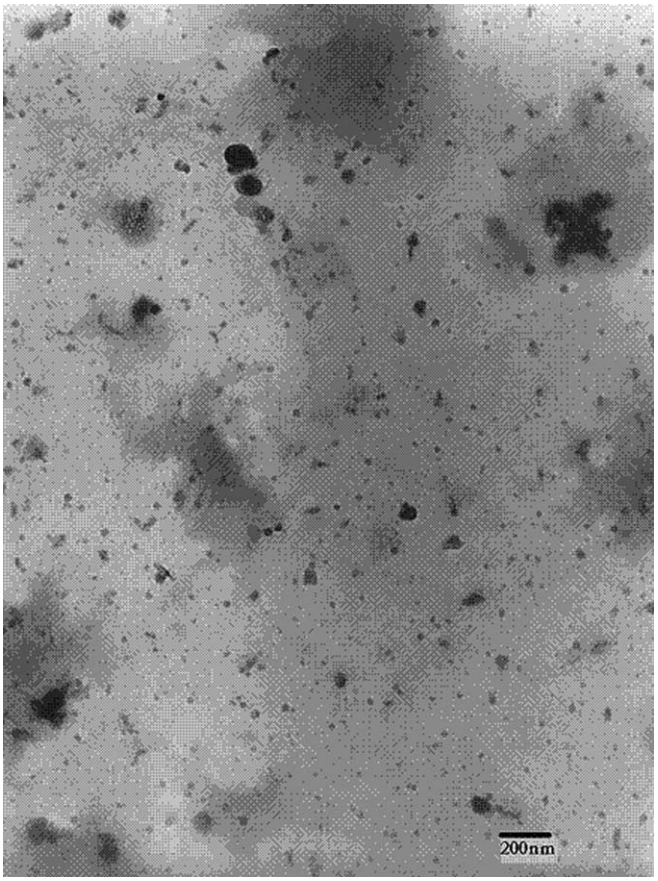

Fig. 7. Transmission electron micrograph of nanoparticles derived from thermolysis of **2b** in refluxing xylene.

the $[Pd(acac)_2]$ complex in presence of trioctylphosphine at 300 °C. EDS results confirmed the presence of palladium in the nanocrystals.

3. Conclusions

Pyrazolate-bridged dimeric allylpalladium(II) complexes $[Pd(\mu\text{-}3,5\text{-}R'_2pz)(\eta^3\text{-}CH_2C(R)CH_2)]_2$ have been synthesised following a facile synthetic approach and characterised. The X-ray structure of **2c**, shows that the dinuclear complex contains two square planar palladium centres bridged by two pyrazole ligands with the coordination of each metal centre completed by allyl substituents, and adopts the conformation in which the allyl groups have an opposite orientation with respect to the Pd_2N_4 core. Their thermal behaviour has also been studied. The complex, $[Pd(\mu\text{-}3,5\text{-}(CF_3)_2pz)(\eta^3\text{-}CH_2C(CH_3)CH_2)]_2$ (**2c**) could be a potential precursor for the deposition of palladium thin films by chemical vapour deposition. The equilibrium vapour pressure of this complex as determined by Knudsen effusion method, could be expressed by the relation: $\ln(p/\mathrm{Pa})(\pm 0.06) = -18047.3/T + 46.85$. Thermolysis of complexes **1b** and **2b** in refluxing xylene (~140 °C) affords palladium nanoparticles having mean sizes between 5 and 12 nm under mild conditions.

4. Experimental

4.1. General experimental details

All the reactions were carried out under an atmosphere of dry argon using standard Schlenk techniques. Solvents were distilled from the appropriate drying agents and degassed before use. The chloro-bridged allylpalladium dimers, $[Pd_2(\mu\text{-}Cl)_2(\eta^3\text{-}C_3H_4R)_2]$ [18], 3,5-diisopropylpyrazole [19], 3,5-di-*tert*-butyl pyrazole [20], 3,5- bis(trifluoromethyl)pyrazole [21] were prepared either by following literature procedures or modifications of them. Thus, in the preparation of $[Pd_2(\mu\text{-}Cl)(\eta^3\text{-}CH_2CHCH_2)]_2$ from K_2PdCl_4 and allyl halide, allyl bromide was used instead of allyl chloride and the reaction mixture was refluxed for 3 h, thereby reducing the reaction time from 24 to 3 h. Melting points were determined in sealed capillaries with an electrothermal melting point apparatus and are uncorrected. C, H, N analyses were carried out with a Thermo Finnigan Flash 1112 series elemental analyser. Infrared spectra were recorded in the range 4000–200 cm^{-1} on a Bomem MB-series FT-IR spectrophotometer as Nujol mulls between polythene sheets. ^1H and $^{13}C\{^1H\}$ spectra were recorded on a Bruker DPX 300 spectrometer. Chemical shifts are referenced to the internal chloroform peak. Thermogravimetric analyses (TGA) were carried out either on a SETARAM 92-16-18 or NETZSCH STA 409 PC/PG instrument. The TG curves were recorded at a heating rate of 10 °C/min under a flow of argon gas. X-ray powder diffraction data were collected on a Philips X-ray diffractometer (Model PW 1729) using Cu Kα radiation (λ 1.54060 Å) at 30 kV and 20 mA. SEM micrographs of the palladium nanocrystals were obtained using a Vega MV2300t/40 scanning electron microscope. Energy dispersive spectroscopy (EDS) analyses were carried out using a Inca Energy

250 instrument coupled to Vega MV2300t/40 scanning electron microscope. Transmission electron microscopy (TEM) was performed using a JEOL 2000 FX electron microscope. The sample of metal nanocrystals was prepared by treating 5 mg of finely ground powder with methanol (15 ml), sonicating the mixture for 10 min, and then applying one drop of the solution to carbon film coated copper grid (300 mesh).

4.1.1. Synthesis of complexes

All the complexes were prepared by using the *acac* method reported by us earlier [13]. The characterization data for the complexes **1b** and **2b** are also reported in Ref. [13]. A typical preparation is described below.

4.1.2. Synthesis of [Pd(μ-3,5-Pr$^i_2$pz)(η^3-CH$_2$C(CH$_3$)CH$_2$]$_2$)

Solid Tl(acac) (0.790 g, 2.60 mmol) was added to a degassed acetonitrile (50 ml) solution of [Pd(μ-Cl)(η^3-CH$_2$)C(CH$_3$)CH$_2$]$_2$ (0.5 g, 1.27 mmol) at 0 °C. After it was stirred for 30 min at 0 °C, an acetonitrile (5 ml) solution of 3,5-Pr^{i}pzH (0.39 g, 2.56 mmol) was added to it. The resulting mixture was stirred at room temperature for 2 h and then filtered through a bed of Celite. The filtrate was evaporated to dryness under reduced pressure and the residue was recrystallised from acetonitrile–ether mixture at −10 °C to obtain complex **2a** as white solid.

4.2. Characterization data for the complexes

4.2.1. Complex **1a**, [Pd(μ-3,5-Pr$^i_2$pz)(η^3-CH$_2$CHCH$_2$)]$_2$

White solid, Yield: 80%. m.p.: 182–184 (*dec*). Anal. Calc. for $C_{24}H_{40}N_4Pd_2$: C, 48.25; H, 6.74; N, 9.37. Found: C, 48.10; H, 6.93; N, 9.23%. IR(cm^{-1}): 1519, 1462, 1376, 1358, 1305, 1290, 1174, 1142, 1133, 1106, 1043, 941, 928, 768, 503. ^{1}H NMR ($CDCl_3$, 300 MHz) δ 1.12–1.33 (m, 24H, HC(C*H*$_3$)$_2$); 2.65 (d, 12.4 Hz), 2.76 (d, 12.4 Hz), 2.80 (d, 12.4 Hz), 2.89 (d, 12.4 Hz) [4H, *anti H*, allyl CH$_2$]; 2.96–3.05 (m, 4H, *H*C-(CH$_3$)$_2$); 3.71 (d, 6.8 Hz), 3.79 (d, 6.8 Hz), 3.81 (d, 6.8 Hz), 3.90 (d, 6.8 Hz) [4H, *syn H*, allyl CH$_2$]; 5.21–5.76 (m, 2H, CH$_2$C*H*CH$_2$). ^{13}C{^{1}H} ($CDCl_3$, 75.47 MHz): δ 22.90 (s), 24.49 (s), 24.73 (s) (HC*C*H$_3$)$_2$,; 29.16 (s) [H*C*-(CH$_3$)$_2$], 55.54 (s), 55.17 (s), 54.86 (s) (allyl *C*H$_2$); 95.41 (s) 95.16 (s), 94.77 (s) (*C*H pz ring); 111.66 (s), 111.92 (s), 113.26 (s), 113.67 (s) (CH$_2$*C*HCH$_2$); 158.65 (s), 159.07 (s), 159.19 (s) (*C*$_3$ + *C*$_5$ pz ring).

4.2.2. Complex **1c**, [Pd(μ-3,5-(CF$_3$)$_2$pz)(η^3-CH$_2$CHCH$_2$)]$_2$

Colourless solid. Yield: 83%. m.p.: 224–226 °C. Anal. Calc. for $C_{16}H_{12}F_{12}N_4Pd_2$: C, 27.41; H, 1.72; N, 7.99. Found: C, 27.24; H, 1.64; N, 8.10%. IR (cm^{-1}): 1527, 1502, 1377, 1253, 1142, 1023, 822, 815, 753, 486. ^{1}H NMR: δ 2.90 (d, 12.4 Hz), 3.03 (d, 12.4 Hz), 3.16 (d, 12.4 Hz), 3.26 (d, 12.4 Hz) (4H, *anti-H*, allyl CH$_2$); 4.06 (d, 6.9 Hz), 4.12 (d, 6.9 Hz), 4.16 (d, 6.9 Hz), 4.24 (d, 6.9 Hz) (*syn-H*, allyl CH$_2$); 5.44–5.84 (m, 2H, CH$_2$C*H*CH$_2$), 6.79 (s), 6.81 (s) [2H, *H*-4 pz ring]. ^{13}C{^{1}H} NMR data: δ 59.80 (s), 60.22 (s), 60.75 (s), 61.10 (s) (allyl *C*H$_2$); 104.74 (s), 114.80 (s) (*C*H pz ring), 115.10 (s), 115.96 (s), 116.58 (s) (CH$_2$*C*HCH$_2$), 120.90 (q, *C*F$_3$, $^1J_{C-F} = 268$ Hz), 121.11 (q, *C*F$_3$, $^1J_{C-F} = 268$ Hz), 142.95 (q, *C*CF$_3$, $^2J_{C-F} = 38$ Hz), 143.10 (q, *C*CF$_3$, $^2J_{C-F} = 38$ Hz).

4.2.3. Complex **2a**, [Pd(μ-3,5-Pr$^i_2$pz)(η^3-CH$_2$C(CH$_3$)CH$_2$)]$_2$

White solid. Yield: 79%. m.p.: 203–206 °C. Anal. Calc. for $C_{26}H_{44}N_4Pd_2$: C, 49.92; H, 7.09; N, 8.95. Found: C, 49.81; H, 7.23; N, 8.79%. IR (cm^{-1}): 1516, 1377, 1358, 1294, 1175, 1142, 1105, 1042, 1020, 921, 897, 835, 764, 476. ^{1}H NMR ($CDCl_3$, 300 MHz): δ 1.16–1.32 (m, 24 H, HC(C*H*$_3$)$_2$); 2.02 (s, 3H, C*H*$_3$ of 2-methylallyl), 2.16 (s, 3H, C*H*$_3$ of 2-methyl allyl); 2.47 (s, 2H, *anti-H*, allyl CH$_2$), 2.72–2.79 (m, 4H, allyl C*H*$_2$ + C*H*(CH$_3$)$_2$); 3.06 (h, 6.9 Hz, C*H*(CH$_3$)$_2$); 5.75 (s, 2H, *H*-4 pz ring). ^{13}C{^{1}H} ($CDCl_3$, 75.47 MHz): δ 22.83 (s), 23.00 (s) (HC(*C*H$_3$)$_2$); 23.46 (s), 23.83 (s) [*C*H$_3$ of 2-methyl allyl]; 24.51 (s), 24.74 (s) (HC(*C*H$_3$)$_2$); 29.21 (s) 29.27 (s) (*C*H(CH$_3$)$_2$), 54.21 (s) 54.66 (s), 54.94 (s), 55.32 (s), (allyl *C*H$_2$), 92.78 (s), 94.80 (s) 95.02 (s) (*C*H pz ring), 127.00 (s), 127.94 (s), 128.28 (s) (CH$_2$*C*HCH$_2$) 158.60 (br, *C*$_3$ + *C*$_5$pz ring).

4.2.4. Complex **2c**, [Pd(μ-3,5-(CF$_3$)$_2$pz)(η^3-CH$_2$C(CH$_3$)-CH$_2$)]$_2$

Colourless solid. Yield: 82%. m.p.: 195–197 °C. Anal. Calc. for $C_{18}H_{16}F_{12}N_4Pd_2$ C, 29.65; H, 2.21; N, 7.68. Found: C, 30.14; H, 1.94; N, 7.82%. IR (cm^{-1}): 1527, 1501, 1261, 1125, 1021, 818, 810, 486. ^{1}H NMR ($CDCl_3$, 300 MHz): δ 2.10 (s, 3H), 2.23 (s, 3H) [C*H*$_3$ of 2-methylallyl], 2.69 (s), 3.09 (s) (*anti-H*, allyl CH$_2$), 3.90 (s), 3.93 (s) (*syn-H*, allyl CH$_2$), 6.79 (s) (2H, *H*-4 pz ring). ^{13}C NMR ($CDCl_3$, 75.47 MHz): δ 22.36 (s) 23.74 (s) [*C*H$_3$ of 2-methylallyl], 58.70 (s), 59.05 (s), 60.15 (s) (allyl *C*H$_2$), 104.69 (s) (*C*-4, pz ring), 121.00 (q, *C*F$_3$, $^1J_{C-F} = 268$ Hz), 121.18 (q, *C*F$_3$, $^1J_{C-F} = 268$ Hz); 130.97 (s) [CH$_2$*C*(CH$_3$)CH$_2$], 132.84 (s), 133.01(s), [CH$_2$*C*(CH$_3$)CH$_2$], 142.94 (q, *C*CF$_3$, $^2J_{C-F} =$ 38 Hz), 143.44 (q, *C*CF$_3$ $^2J_{C-F} = 38$ Hz).

4.3. Vapour pressure measurements

The vapour pressure of the **2c** was determined by measuring its partial pressure in the temperature range 359–385 K, using Knudsen effusion mass loss technique. The vapour pressure data for **2c** were generated by monitoring the rate of mass loss of the sample under isothermal conditions with the help of a thermobalance (SETARAM, Model B24). A detailed description of the apparatus and the procedure for the data collection has been described elsewhere [22] The mass calibration of the micro-balance was done using standards weights at room temperature. The temperature calibration for the sample was done by the drop method [23], using high-purity indium metal as standard.

About 200 mg of powdered sample was put in a perfectly degassed graphite cup inside the Knudsen cell of 15 mm diameter and 15 mm height, having a circular knife edged orifice of diameter 0.5 mm. In order to ensure the quick equilibrium between sample and its vapour products, the sample was well spread in the crucible so that ratio of the projected surface of sample to the orifice is high (about 50). The vapour pressures were measured both in ascending and descending mode of temperatures to ensure the absence of kinetic impediments of the vapour generation inside the cell.

The rate of mass loss from the Knudsen cell was measured for the sample at different temperatures. The observed reproducibility in the mass loss rate in each isothermal run in ascending or descending orders of temperature fixation confirms the absence of kinetic hindrance in the evaporative loss. Several measurements were carried out in the range of temperature 359–385 K over the sample.

4.4. Crystallography

Intensity data for **2c** were measured at 223 K on a Enraf Nonius FR590 diffractometer employing Mo Kα radiation so that $\theta_{max} = 25.0°$. The structure was solved by heavy-atom methods [24] and refinement anisotropic displacement parameters, hydrogen atoms in the riding model approximation and a weighting scheme of the form $w = 1/[\sigma^2(F_o^2) + (0.023P)^2 + 2.086P]$ for $P = (F_o^2 + 2F_c^2)/3$ was on F^2 [25]. Positional disorder was noted in the structure so that two positions were resolved for the CF_3 groups bound to the C6b and C7b atoms. The major component (anisotropic refinement) had a site occupancy = 0.934(6). The molecular structure, shown in Fig. 2, was drawn with ORTEP [26] at 25% probability ellipsoids. Data manipulation were performed using TEXSAN [27]. The refinement converged to final R [for 3712 reflections with $I > 2(I)$] = 0.021 and $wR = 0.052$ (all 4236 data)]. *Crystal data*: $C_{18}H_{16}F_{12}N_4Pd_2$, $M = 729.15$, monoclinic, space group $P2_1/n$, $a = 14.485(3)$, $b = 12.1112(8)$, $c = 15.437(2)$ Å, $\beta = 117.21(1)°$, $V = 2408.4(6)$ Å^3, $Z = 4$, $D_c = 2.011$ g/cm^3, $\mu = 1.600$ mm^{-1}, $F(000) = 1408$.

A preliminary crystallographic examination was also conducted on complex **1b**, isolated as its 1:1 acetonitrile adduct. The structure was found to be badly distorted, even at −50 °C, which precluded a complete determination and so full details are not reported here (see Section 2). *Crystal data*: $C_{30}H_{51}N_5Pd_2$, $M = 694.56$, orthorhombic, space group *Pbca*, $a = 10.343(3)$, $b = 18.802(3)$, $c = 33.927(6)$ Å, $V = 6598(2)$ Å^3, $Z = 8$.

4.5. Thermolysis procedure

Bulk thermolyses of **1a** and **2a** at 500 °C were performed by heating 0.5 g of **1a** and **2a** in a quartz boat at a rate of 5 °C min^{-1} from 25 to 500 °C under high-purity argon. Once at 500 °C, an isotherm was maintained for 2 h before allowing the sample to cool to room temperature. The products for both **1a** and **2a** were black shiny powders. The typical yields obtained were 84% (**1a**) and 88% (**2a**) respectively. Bulk thermolyses of **1b** and **2b** were conducted by refluxing a xylene solution of **1b** and **2b** (0.6 g in 40 ml of xylene) for 1 h under an argon atmosphere. A shiny black powder separated in both the cases. The resulting suspension was centrifuged to obtain the black powder which was washed with diethyl ether (3 × 2 ml) and dried in air. The typical yields obtained were 40% (**1b**) and 68% (**2b**).

5. Supplementary material

Crystallographic data for the structural analysis has been deposited with the Cambridge Crystallographic Data Centre, CCDC no. 287140 for compound **2c**. Copies of this information may be obtained free of charge from The Director, CCDC, 12 Union Road, Cambridge CB2 1EZ, UK (Fax: +44 1223 336033; e-mail: deposit@ccdc.ac.uk or www: http://www.ccdc.cam.ac.uk).

Acknowledgements

The authors thank Drs. S.K. Gupta and Shovit Bhattacharya for SEM and EDS analysis. The authors also thank Dr. R.K Singhal and Dr. G.K. Dey for providing microanalyses of the samples and TEM analysis, respectively.

References

[1] P.D. Gurney, R.J. Seymour, in: F.R. Hartley (Ed.), Chemistry of Platinum Group Metals, Elsevier, Oxford, UK, 1991.
[2] L. Sordelli, G. Martra, R. Psaro, C. Dossi, S. Coluccia, J. Chem. Soc., Dalton Trans. (1996) 765.
[3] (a) G. Saracco, V. Specchia, Catal. Rev. Sci. Eng. 36 (1994) 305;
(b) J.N. Armor, Catal. Today 25 (1995) 199.
[4] (a) A. Beck, A. Horváth, A. Sárkány, L. Guczi, in: Z. Bing, S. Hermans, G.A. Somorjai (Eds.), Nanotechnology in Catalysis, vol. 1, Springer, Berlin, 2004, pp. 83–110 (Chapter 5);
(b) S.U. Son, Y. Yang, J. Park, H.B. Na, H.M. Park, H.J. Yun, J. Lee, T. Hyeon, J. Am. Chem. Soc. 126 (2004) 5026.
[5] (a) A.A. Zinn, L. Brandt, H.D. Kaesz, R.F. Hicks, in: T.T. Kodas, M.J. Hampden-Smith (Eds.), The Chemistry of Metal CVD, VCH, Weinheim, Germany, 1994;
(b) J.E. Gozum, D.M. Pollina, J.A. Jensen, G.S. Girolami, J. Am. Chem., Soc. 110 (1988) 268.
[6] Y. Zhang, Z. Yuan, R.J. Puddephatt, Chem. Mater. 10 (1998) 2293.
[7] Y.L. Tung, W.C. Tseng, C.Y. Lee, P.F. Hsu, Y. Chi, S.M. Peng, G.H. Lee, Organometallics 18 (1999) 864.
[8] S. Trofimenko, Chem. Rev. 72 (1972) 497;
S. Trofimenko, Prog. Inorg. Chem. 34 (1986) 115.
[9] (a) G. La Monica, G.A. Ardizzoia, Prog. Inorg. Chem. 46 (1997) 151;
(b) A.P. Sadimenko, S.S. Basson, Coord. Chem. Rev. 147 (1996) 247;
(c) J.E. Cosgriff, G.B. Deacon, Angew. Chem., Int. Ed. Engl. 37 (1998) 286.
[10] (a) D. Pfeiffer, M.J. Heeg, C.H. Winter, Inorg. Chem. 39 (2000) 2377;
(b) C.H. Winter, P.J. Mckarns, J.T. Scheper, Mater. Res. Soc. Symp. Proc. 495 (1998) 95;
(c) C.H. Winter, J.L. Sebestl, M.J. Heeg, Mater. Res. Soc. Symp. Proc. 495 (1998) 147;
(d) D. Pfeiffer, M.J. Heeg, C.H. Winter, Angew. Chem., Int. Ed. Engl. 37 (1998) 2517.

[11] (a) J.G. Cederberg, T.D. Culp, B. Bieg, D. Pfeiffer, C.H. Winter, K.L. Bray, T.F. Kuech, J. Appl. Phys. 85 (1999) 1825;
(b) D. Pfeiffer, B.J. Ximba, L.M. LiableSandes, A.L. Rheingold, M.J. Heeg, D.M. Coleman, H.B. Schlegel, T.F. Kuech, C.H. Winter, Inorg. Chem. 38 (1999) 4539;
(c) C.L. Dezelah IV, O.M. El-Kadri, M.J. Heeg, C.H. Winter, J. Mater. Chem. 14 (2004) 3167.
[12] Z. Wang, C.D. Abernethy, A.H. Cowley, J.N. Jones, R.A. Jones, C.L.B. Macdonald, L. Zhang, J. Organomet. Chem. 666 (2003) 35.
[13] A. Singhal, J. Chem. Res.(S) (2005) 702.
[14] S. Trofimenko, Inorg. Chem. 10 (1971) 1372.
[15] G.W. Henslee, J.D. Oliver, J. Cryst. Mol. Struct. 7 (1977) 137.
[16] Joint Committee on Powder Diffraction Standards (JCPDS) card No. 5-681.
[17] S.-W. Kim, J. Park, Y. Jang, Y. Chung, S. Hwang, T. Hyeon, Y.W. Kim, Nano Lett. 3 (2003) 1289.
[18] R.C. Palenik, G.J. Palenik, Synth. React. Inorg. Met-Org. 22 (1992) 1395.
[19] N. Kitajima, K. Fujisawa, C. Fujimoto, Y. Moro-oka, S. Hashimoto, T. Kitagawa, K. Tatsumi, A. Nakamura, J. Am. Chem. Soc. 114 (1992) 1277.
[20] C. Fernández-Castaño, C. Foces-Foces, N. Jagerovic, J. Elguero, J. Mol. Struct. 355 (1995) 265.
[21] (a) S. Trofimenko, J. Am. Chem. Soc. 89 (1967) 3165;
(b) O. Renn, L.M. Venanzi, A. Marteletti, V. Gramlich, Helv. Chim. Acta 78 (1995) 993.
[22] R. Mishra, S.R. Bhardwaj, D. Das, J. Nucl. Mater. 321 (2003) 318.
[23] O. Kubaschewski, C.B. Alcock, P.J. Spencer, Metallugical Thermochemistry, sixth ed., Pergamon Press, Oxford, 1993.
[24] G.M. Sheldrick, *SHELXS-97*, Program for the Solution of Crystal Structures, University of Göttingen, Germany, 1997.
[25] G.M. Sheldrick, *SHELXL-97*. Program for Crystal Structure Refinement, University of Göttingen, Germany, 1997.
[26] C.K. Johnson, ORTEPII. Report ORNL-5138, Oak Ridge National Laboratory, TN, 1976.
[27] TEXSAN: Single Crystal Structure Analysis Software. Molecular Structure Corporation, The Woodlands, TX, Version 1.7, 1997.